Directionally induced hydrogen bonding interactions of heteroatom-incorporated amine adsorbents for promoting steady CO_2 capture

Li Lin [a], Yuan Meng [b], Jinglin Li [a], Kailun Chen [a], Endian Hu [a], Jingwen Chang [a], Yuchen Gao [a], Jianguo Jiang [a*]

[a] School of Environment, Tsinghua University, Beijing 100084, China

[b] Department of Civil and Environmental Engineering, The Hong Kong Polytechnic University, Hung Hom, Kowloon, Hong Kong, China

*** Corresponding author:** Email: jianguoj@tsinghua.edu.cn (J. Jiang)

1 Experimental section

1.1 Preparation of metal-incorporated silica and amine-impregnated adsorbents

PEI (99%) with 600 Da molecular weight was purchased from Adamas (China), and SBA-15 (primary pore diameter: 6-11 nm) was purchased from XFNANO (China). Methanol (HPLC grade) was purchased from Fisher Scientific (USA), and ethanol (AR) was purchased from Greagent (China). $Al(NO_3)_3 \cdot 9H_2O$ (AR) and $Fe(NO_3)_3 \cdot 9H_2O$ (AR) were purchased from Aladdin (China), while $Ce(NO_3)_4$ (AR) was purchased from Boer (China). Nitrogen (N_2; 99.999%) and CO_2 (99.999%) were purchased from Praxair (USA).

The metal-incorporated silica had been prepared by the impregnation method. Firstly, bare silica was degassed in an oven under vacuum (pressure $<$ 1 mmHg) at 105 ℃ for 3 h. Then, the required amount of metal nitrate was dissolved in 20 mL of ethanol and stirred until completely mixed at room temperature. Subsequently, 1 g of degassed silica and another 15 mL of ethanol were added. The mixture was stirred at 40 ℃ overnight until the solvent had almost completely evaporated. The residue was dried under vacuum at 60 ℃ for 3 h. Finally, the product was calcined at 550 ℃ for 4 h. The metal-incorporated silica was named SBA-15-Me, where Me referred to the type of metal (Me = Al, Ce, Ce', Fe, or Fe'). Wherein the amount of substance ratio of metal and silica in SBA-15-Al, SBA-15-Ce, and SBA-15-Fe were 3.33%, while the mass ratio

of metal and silica in SBA-15-Al, SBA-15-Ce', and SBA-15-Fe' were 1.50%. This referred to the proportion added during preparation. Therefore, SBA-15-Al, SBA-15-Ce, and SBA-15-Fe could compare the effects of adding different types of metals on the performance of adsorbents. SBA-15-Ce', and SBA-15-Fe' provided additional explanation on the effects of metal quality.

The preparation method of solid amine adsorbents had been previously reported by our group's paper [1]. Firstly, the required amount of amine was dissolved in 20 mL of methanol and stirred until completely mixed at room temperature. Subsequently, 1 g of degassed silica or metal-incorporated silica and another 10 mL of methanol were added. The mixture was stirred at 40 ℃ for 12 h until the solvent had almost completely evaporated. Finally, the residue was dried under vacuum at 50 ℃ for 4-5 h and the final product was collected for analysis. The synthesized amine-impregnated adsorbents were named SBA-15-N or SBA-15-Me-N, where Me referred to the type of metal (Me = Al, Ce, Ce', Fe, or Fe').

1.2 Characterization

The chemical groups of the samples were determined by Fourier transform infrared spectroscopy (FTIR) using an infrared spectrometer (Thermo Scientific, USA). The resolution and scan frequency were 4.0 cm^{-1} and 64 min^{-1}, respectively.

The thermal stabilities of the samples were measured by thermogravimetric analysis (TGA) using a TGA/DSC 2 STAR^e thermogravimetric analyzer (Mettler Toledo, USA).

The analysis was conducted from 30 ℃ to 900 ℃ at a rate of 10 ℃/min under a 100 mL/min N_2 flow.

The contents of carbon (C), hydrogen (H), and nitrogen (N) in the solid amine adsorbents were measured using a Vario EL III Elemental Analyzer (Elementar, Germany). Two replicate samples were analyzed for each product. The amine loadings of the adsorbents were calculated according to the results of elemental analysis, approximating by subtracting the sum of the contents of C, H, and N in bare silica from the sum of the contents of C, H, and N in solid amine adsorbents.

The metal contents in the solid amine adsorbents were measured by inductively coupled plasma-optical emission spectrometry (Thermo Scientific, USA). The samples were digested into solution before testing.

The pore characteristics of the samples were determined using an ASAP 2020 system (Micromeritics, USA). Bare silica and metal-incorporated ones were degassed under vacuum for 5 h at 110 ℃. The PEI-modified samples were degassed for 9 h at 50 ℃. Then N_2 adsorption-desorption isotherms were collected at -196 °C, and the specific surface areas were obtained through the Brunauer-Emmett-Teller (BET) model, while the pore distributions were obtained based on the Barrett-Joyner-Halenda (BJH) model.

Powder X-ray diffraction (XRD) pattern was performed on a D8 Advance diffractometer (Bruker, Germany) using a Cu Kα radiation. The diffraction data were recorded in the 2θ range of 10–90° with a scanning speed of 5°/min and 0.5–5° with a scanning speed of 1°/min.

X-ray photoelectron spectroscopy (XPS) results were obtained with a K-Alpha electron spectrometer (Thermo Scientific, USA) using Al-Kα radiation.

The contents of OH groups in the samples were determined by in-situ diffuse reflectance infrared Fourier transform spectroscopy (in-situ DRIFTS) using an in-situ infrared spectrometer (Thermo Scientific, USA). A certain amount of the sample was placed in the in-situ reaction cell and first degassed for 0.5 h at 120 ℃ under a 50 mL/min N_2 flow. Then, the temperature was switched to room temperature, collecting the spectrum as the background. Finally, the gas was switched to a 50 mL/min 10%NH_3/He flow for 0.5 h and the spectrum was collected. The resolution and scan frequency were 4.0 cm^{-1} and 64 min^{-1}, respectively.

1.3 Adsorption and cyclic experiment

The CO_2 adsorption measurements were performed using a TGA/DSC 2 STAR^e thermogravimetric analyzer. A certain amount of the sample was placed in the oven and first degassed for 0.5 h at 120 ℃ under a 60 mL/min N_2 flow. Then the temperature was decreased to the adsorption temperature (40, 60, 80, 100, and 120 ℃) and the gas was switched to a 60 mL/min CO_2 flow for 1 h. The CO_2 adsorption capacity was calculated from the thermogravimetric (TG) curves.

The cyclic stability was measured firstly under the same degasification conditions. In the adsorption process, the temperature was decreased to 100 ℃, and the gas was switched to a 60 mL/min CO_2 flow for 0.5 h. In the desorption process, the temperature was increased to 120/150 ℃, and the gas was switched to a 60 mL/min N_2 flow for 0.5

h. The adsorption/desorption cycles were conducted 30 times. In this study, 30 adsorption-desorption cycles were performed on the amine-impregnated adsorbents under two conditions (condition 1: adsorption at 100 °C within a CO_2 flow for 30 min and desorption at 120 °C within a N_2 flow for 30 min; condition 2: adsorption at 100 °C within a CO_2 flow for 30 min and desorption at 150 °C within a N_2 flow for 30 min) and the CO_2 uptakes of each cycle were recorded. What's more, FTIR results were also recorded after 30 adsorption-desorption cycles to reflect the formation of urea.

1.4 Breakthrough experiment

The breakthrough measurements were performed using a fixed-bed system. A certain amount of the sample was placed in the reactor and first degassed for 1 h at 120 ℃ under a 50 mL/min N_2 flow. Then the temperature was decreased to 100 ℃ and the gas was switched to a 50 mL/min 15%CO_2/85%N_2 flow for 1 h. The outlet concentrations of CO_2 and N_2 were measured using an online Micro-490 gas chromatography (Agilent, USA) equipped with a thermal conductivity detector. The breakthrough and saturation capacity of CO_2 was obtained from the dynamic CO_2 breakthrough curve, calculated as follows:

$$q_b = \frac{Qc_0\left[\int_0^{t_b}\left(1-\frac{c_t}{c_0}\right)dt - t_D\right]}{m \cdot V_m} \times \frac{T_0}{T} \times M_w \quad (1)$$

$$q_s = \frac{Qc_0\left[\int_0^{t_s}\left(1-\frac{c_t}{c_0}\right)dt - t_D\right]}{m \cdot V_m} \times \frac{T_0}{T} \times M_w \quad (2)$$

where q_b was the breakthrough capacity of CO_2, mg/g; q_s was the saturation capacity

of CO_2, mg/g; m was the mass of the sorbent packed in the bed, g; Q was the feed flow rate, mL/min; c_0 was the initial CO_2 concentration in feed mixture, %; c_t was the CO_2 concentration at the outlet of the column, %; t_D was the dead time of fixed-bed, 0.667 min; T_0 was the temperature in standard condition, 273.15 K; T was the adsorption temperature, K; M_w was the molar mass of CO_2, 44.0095 g/mol; V_m was the molar gas volume in standard condition, 22.4 L/mol; t_b was the breakthrough time at which c_t reached 5% of c_0, min; t_s was the exhaustion time at which c_t reached 95% of c_0, min [2].

2 Supporting figures

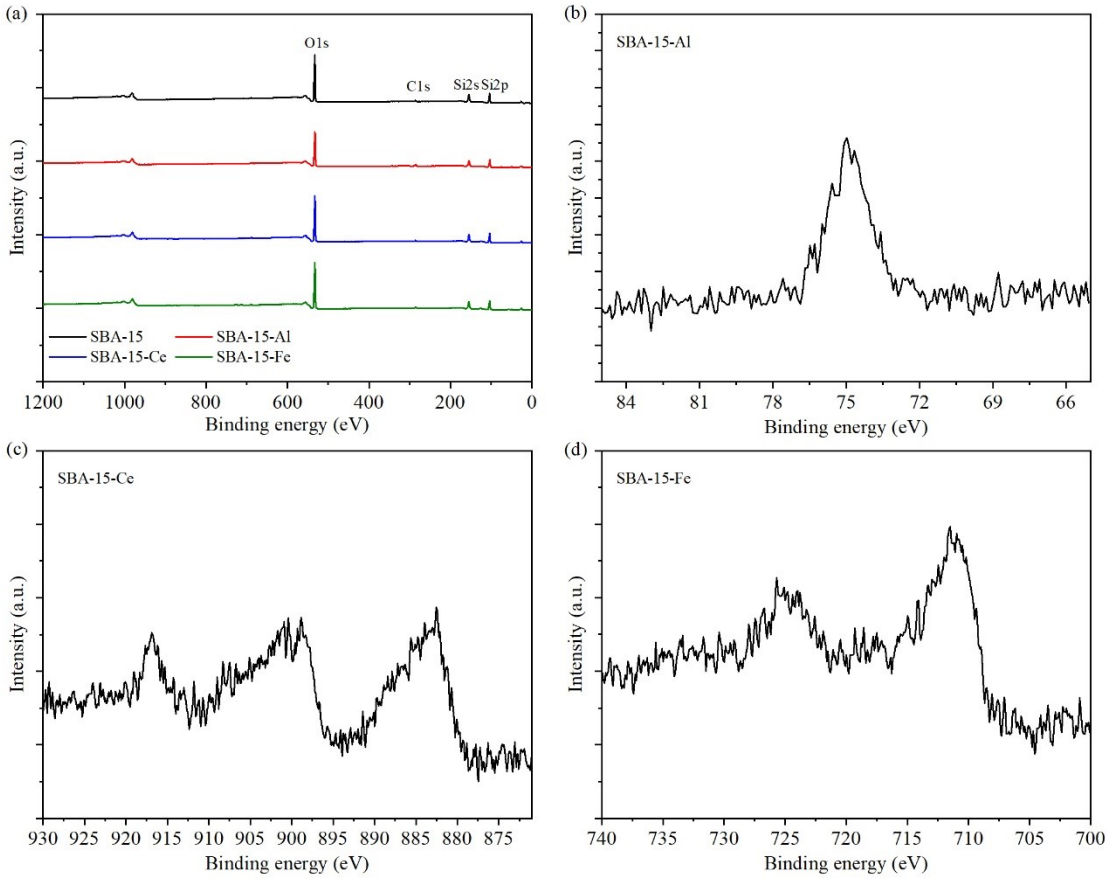

Figure S1. (a) the survey scan XPS spectra of SBA-15 and metal-incorporated silica; (b) Al2p high-resolution XPS spectra of SBA-15-Al-N; (c) Ce3d high-resolution XPS spectra of SBA-15-Ce-N; (d) Fe2p high-resolution XPS spectra of SBA-15-Fe-N.

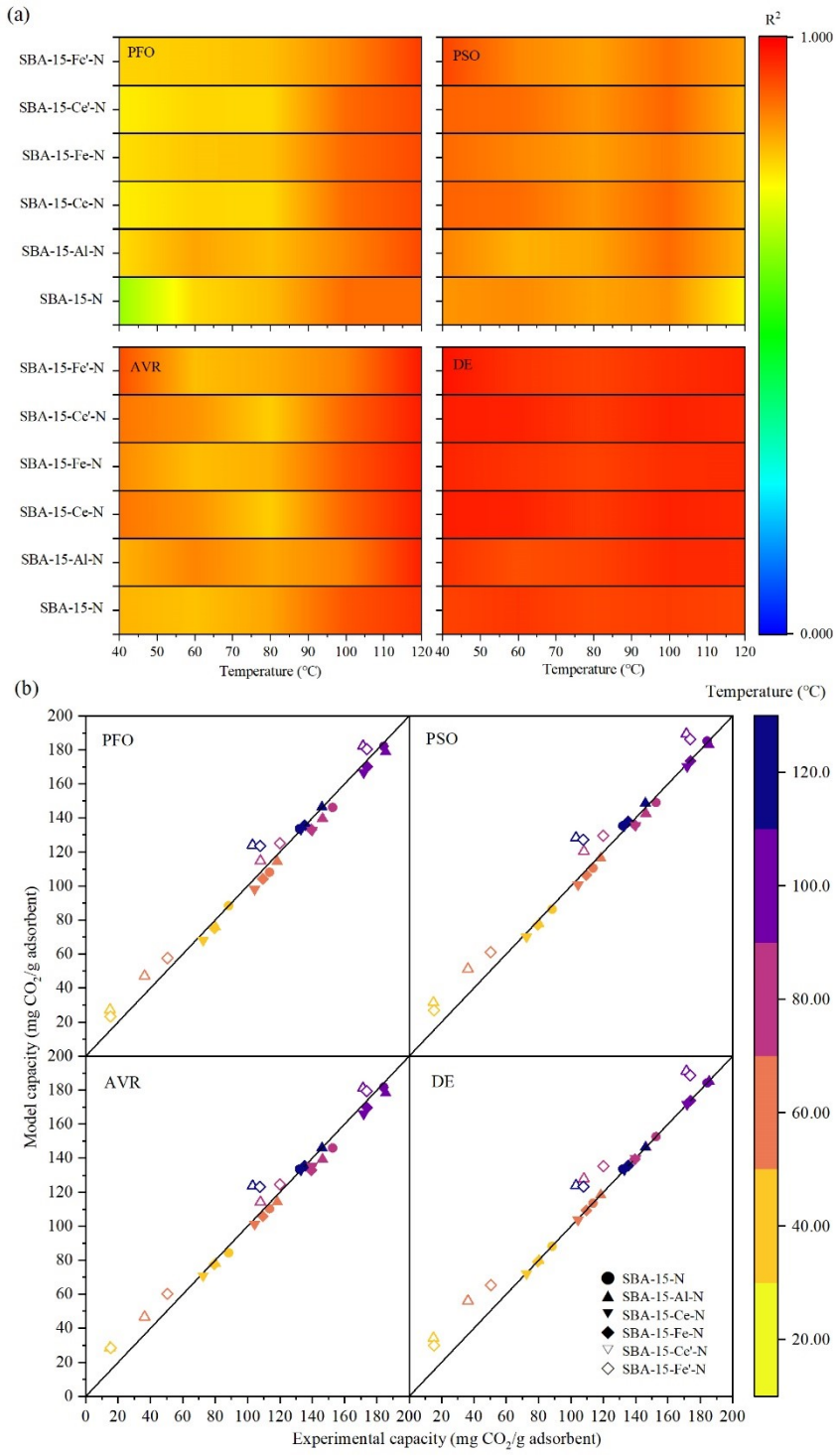

129

130 **Figure S2. (a) R^2 values of different models and (b) Parity plots for different models applied**

131 **to amine-impregnated adsorbents.**

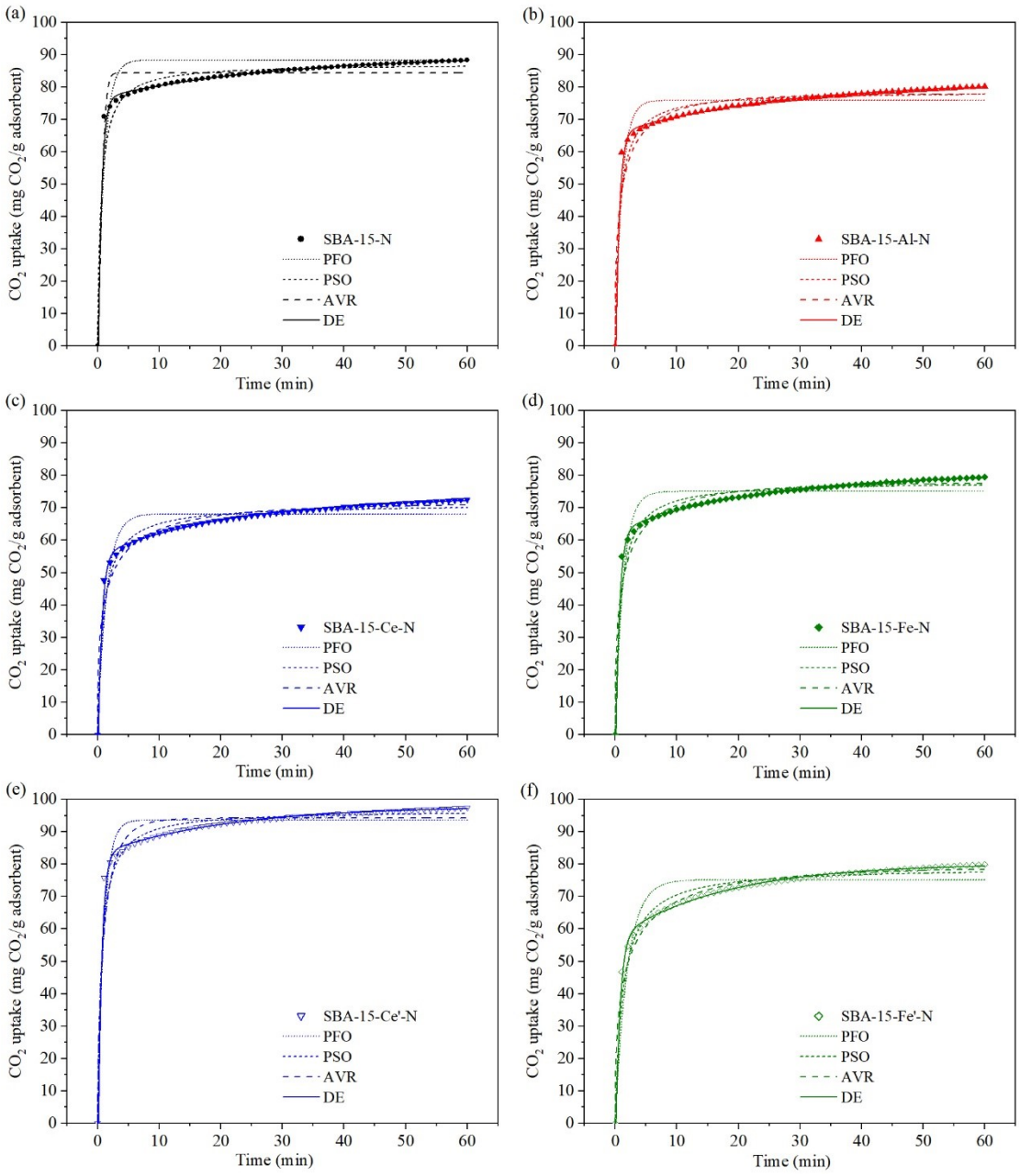

132

133 **Figure S3. Adsorption curves of amine-impregnated adsorbents at 40 °C.**

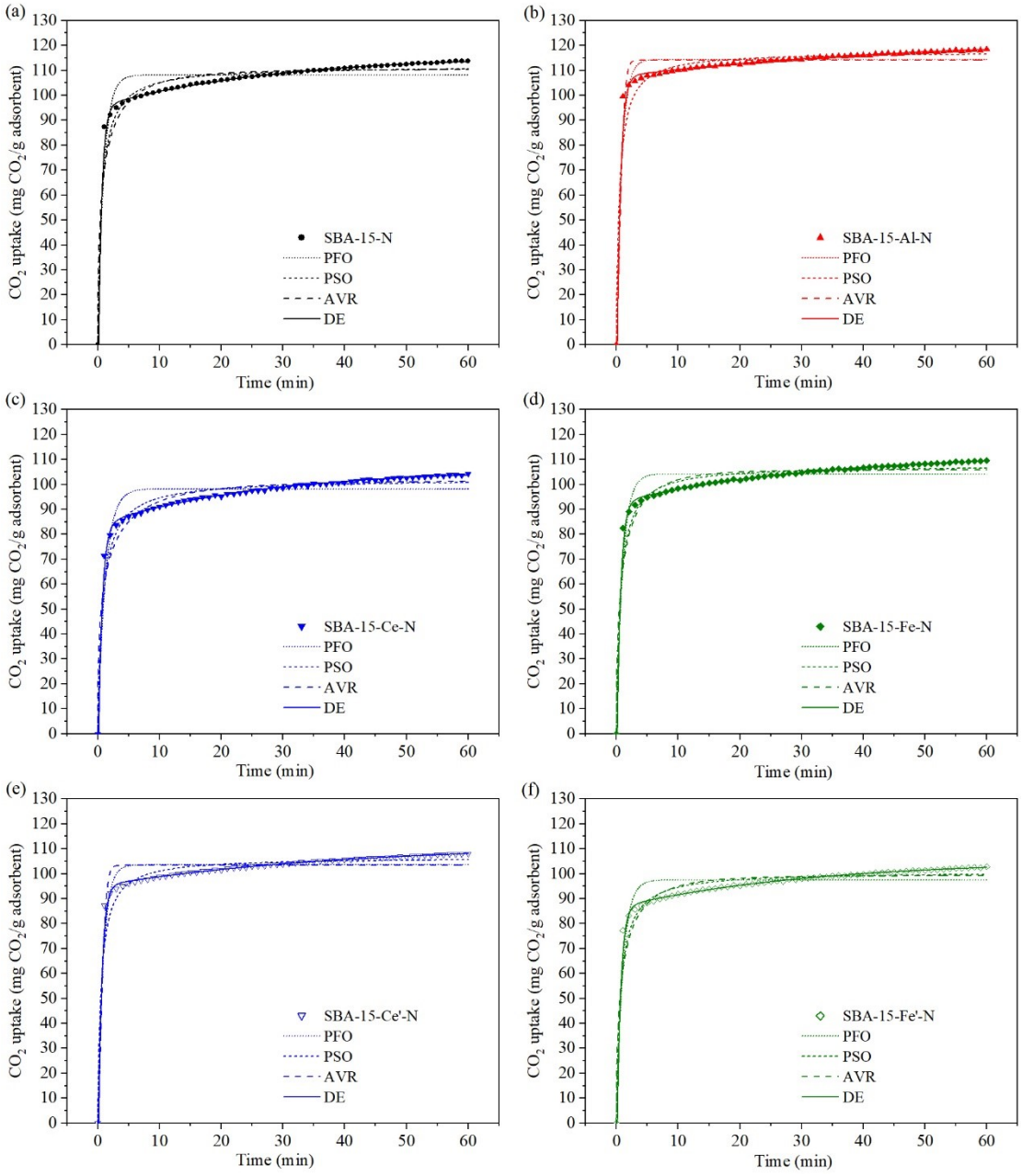

134

135 **Figure S4. Adsorption curves of amine-impregnated adsorbents at 60 °C.**

136

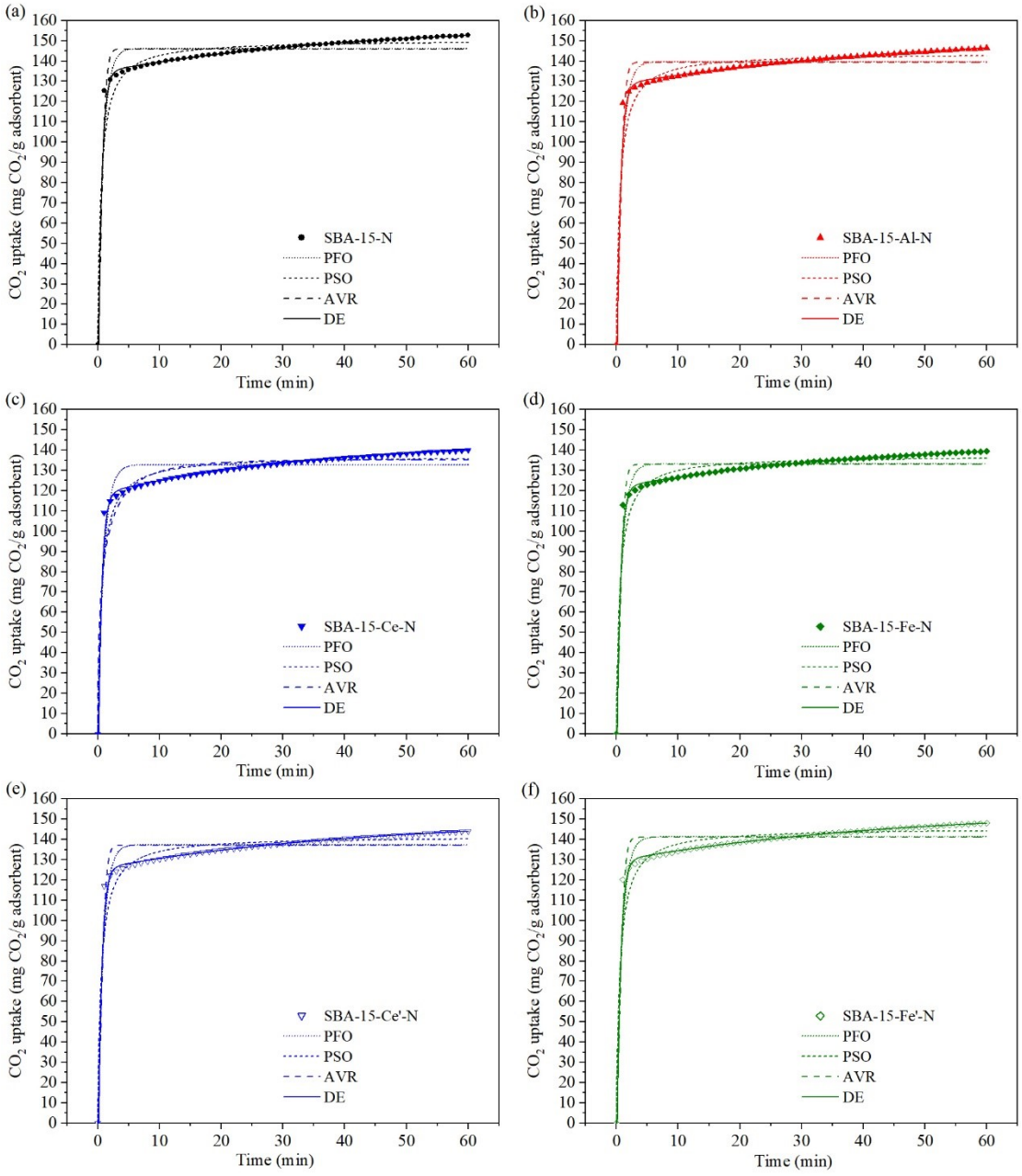

137

138 **Figure S5. Adsorption curves of amine-impregnated adsorbents at 80 °C.**

139

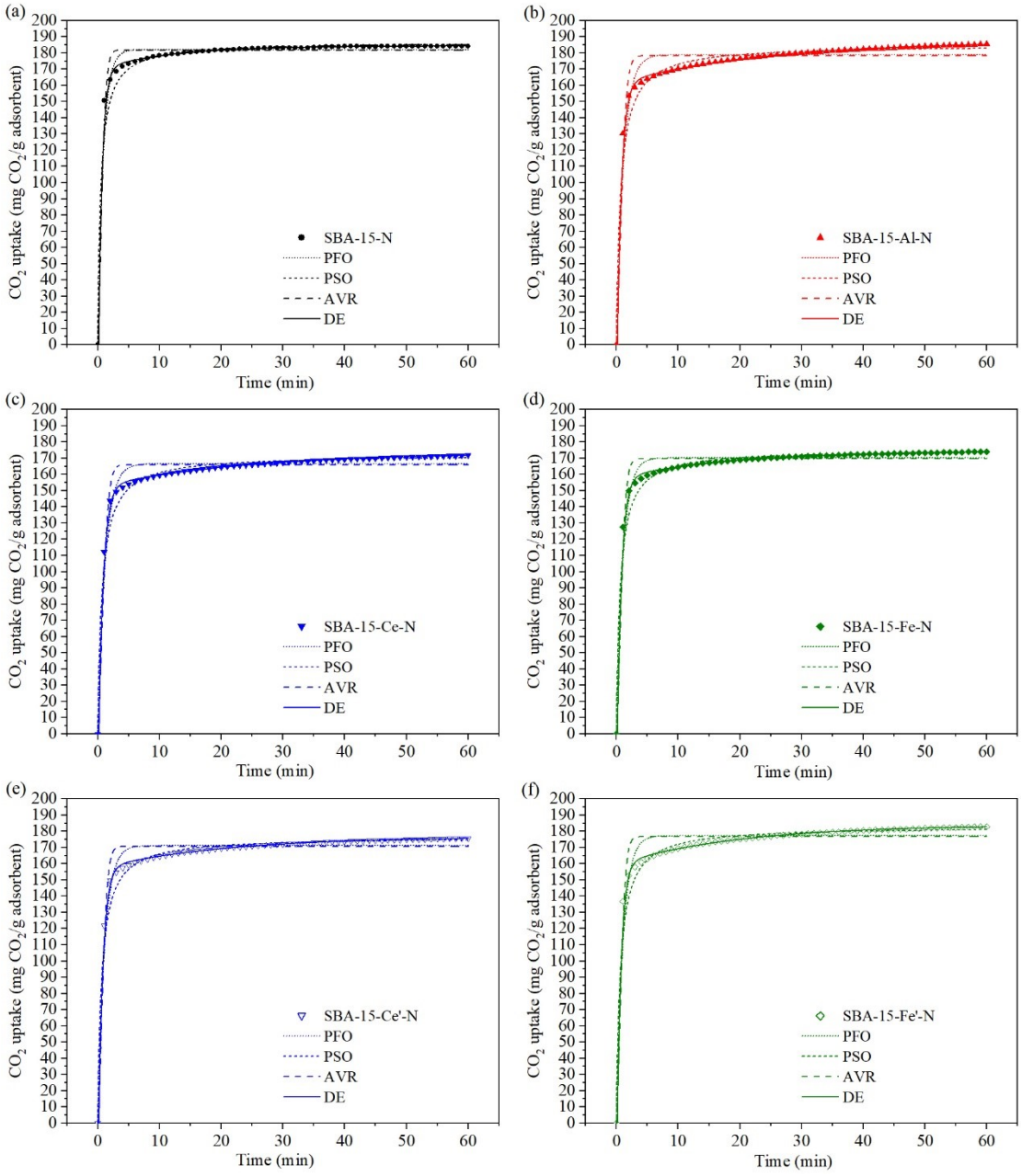

140

141 **Figure S6. Adsorption curves of amine-impregnated adsorbents at 100 °C.**

142

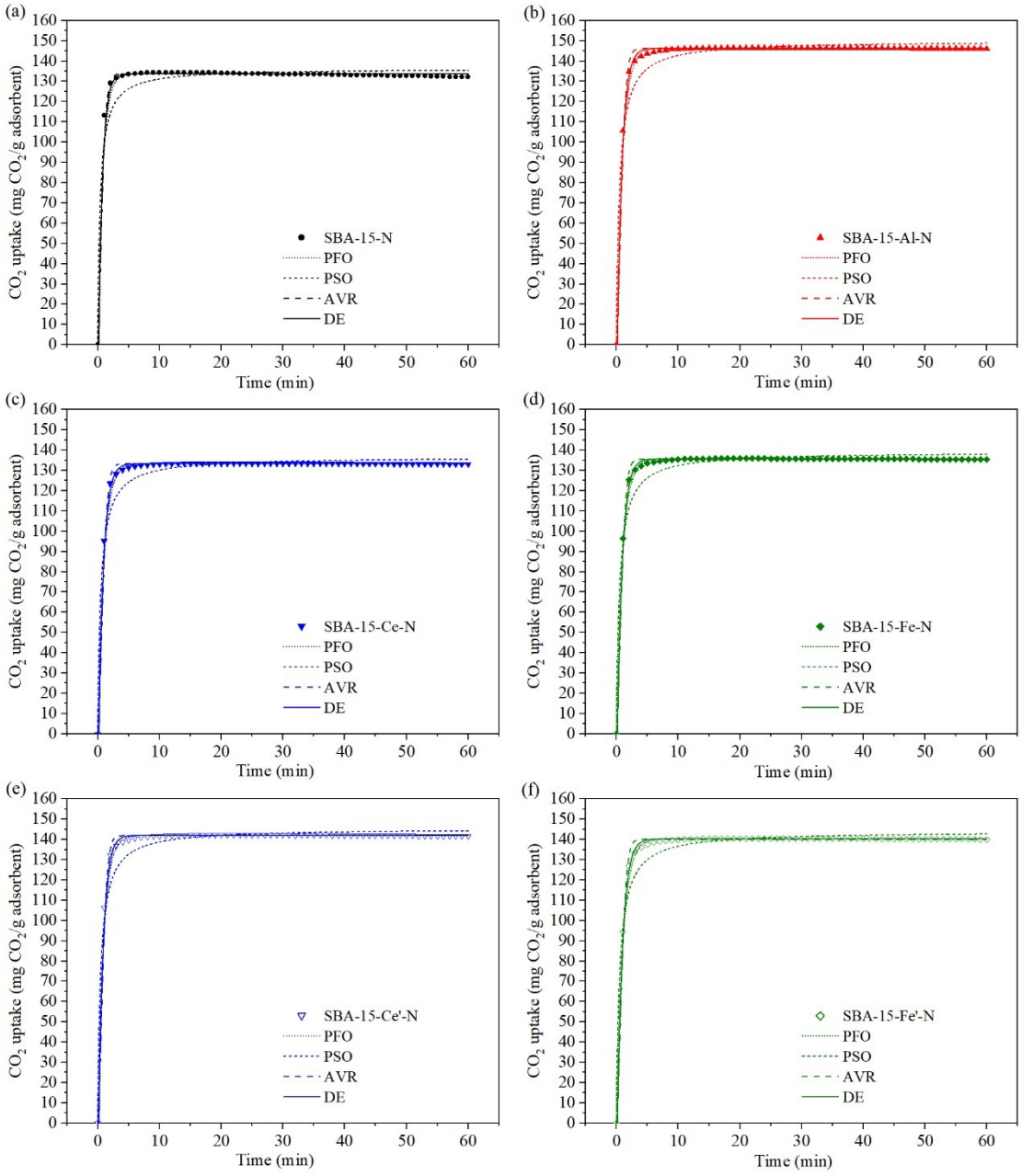

143

144 **Figure S7. Adsorption curves of amine-impregnated adsorbents at 120 °C.**

145

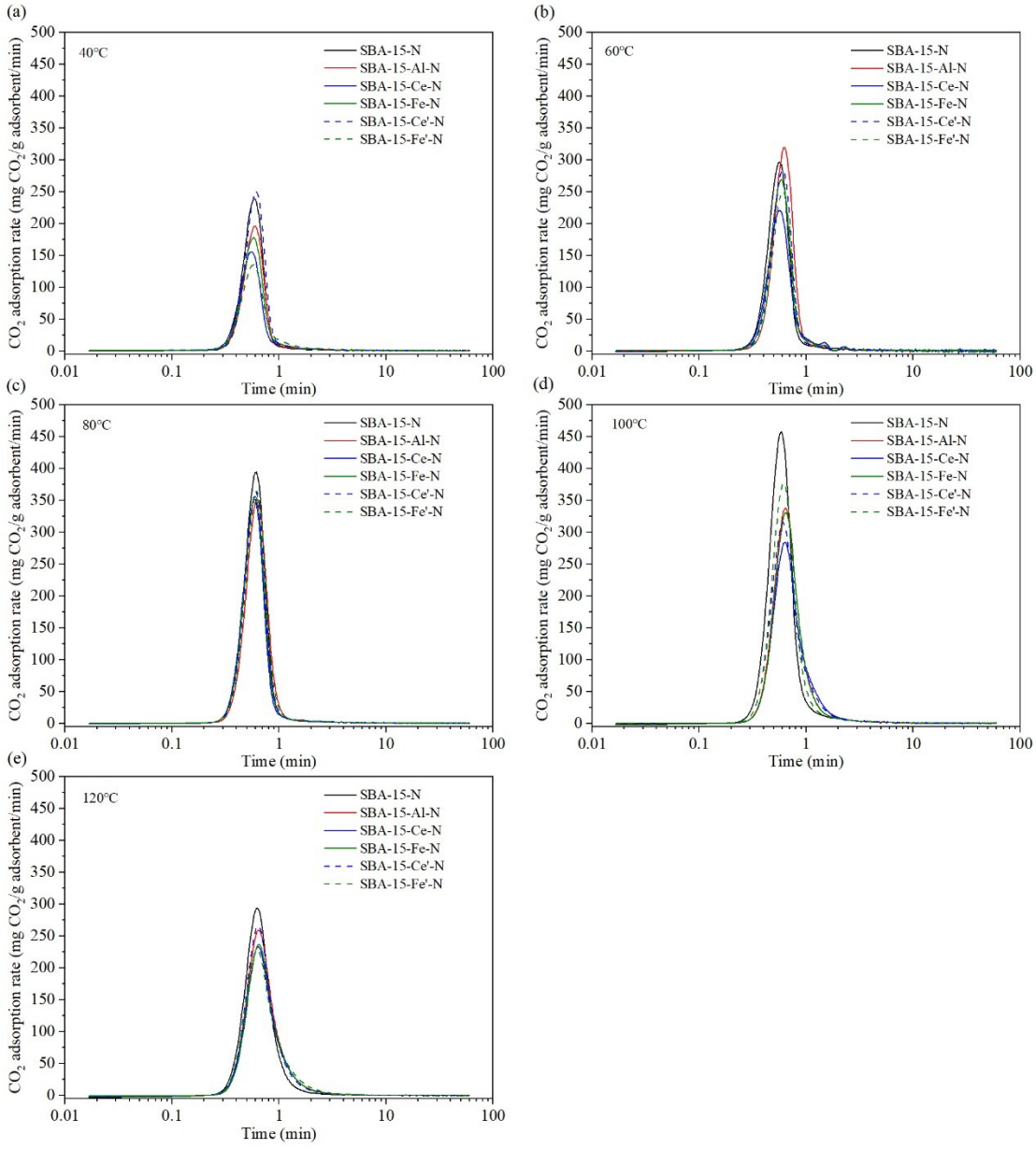

Figure S8. CO_2 adsorption rates of amine-impregnated adsorbents at different temperatures.

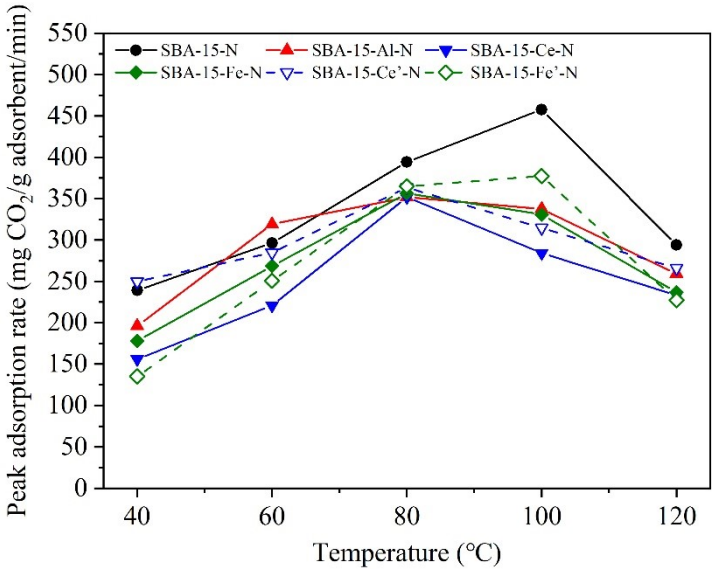

148

149 **Figure S9. Peak adsorption rates of amine-impregnated adsorbents.**

150

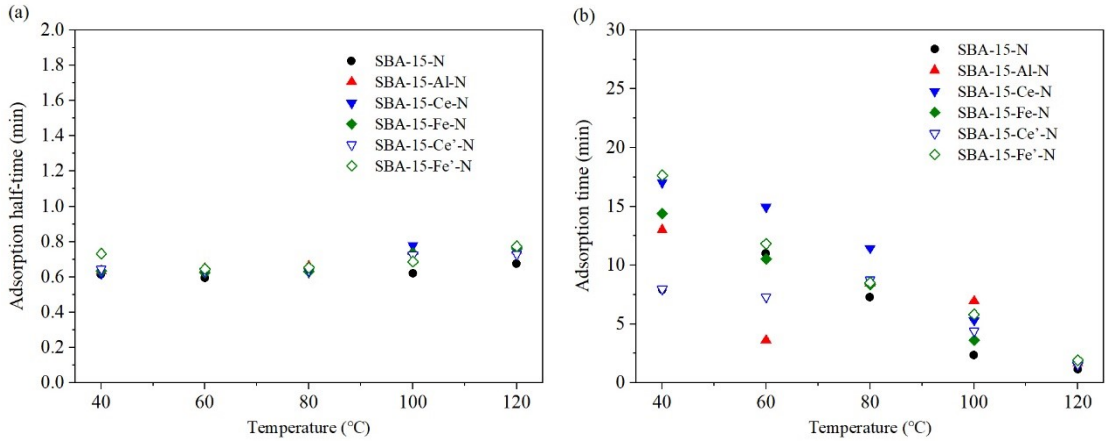

151

152 **Figure S10. (a) adsorption half-times of amine-impregnated adsorbents; (b) adsorption time**

153 **lengths for 90% CO_2 uptakes of amine-impregnated adsorbents.**

154

155

156

157

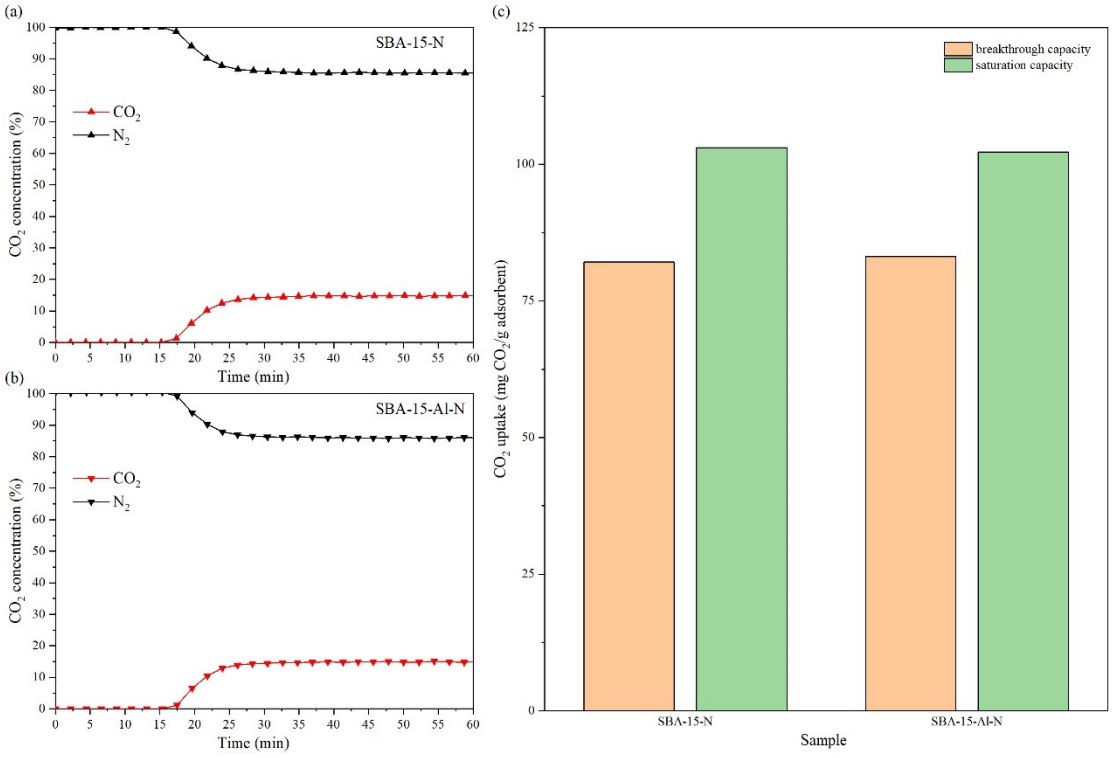

158

159 **Figure S11. Breakthrough measurements using (a) SBA-15-N and (b) SBA-15-Al-N at 100 °C**

160 **under a 15%CO_2/85%N_2 flow; (c) CO_2 breakthrough and saturation capacities calculated**

161 **from CO_2 breakthrough curves.**

162 Breakthrough experiments under a 15%CO_2/85%N_2 flow were conducted to find the

163 actual effect of the flue gas. The metal-incorporated adsorbent represented by SBA-15-

164 Al-N had a breakthrough capacity of 83.11 mg/g and a saturation capacity of 102.27

165 mg/g, which were similar to those of SBA-15-N (Figure S11). Compared with other

166 solid amine adsorbents applied to similar conditions [3, 4], the metal-incorporated

167 adsorbent synthesized in this work exhibited excellent breakthrough and saturation

168 capacity, which was expected to be applied to carbon capture in actual flue gas.

169

170

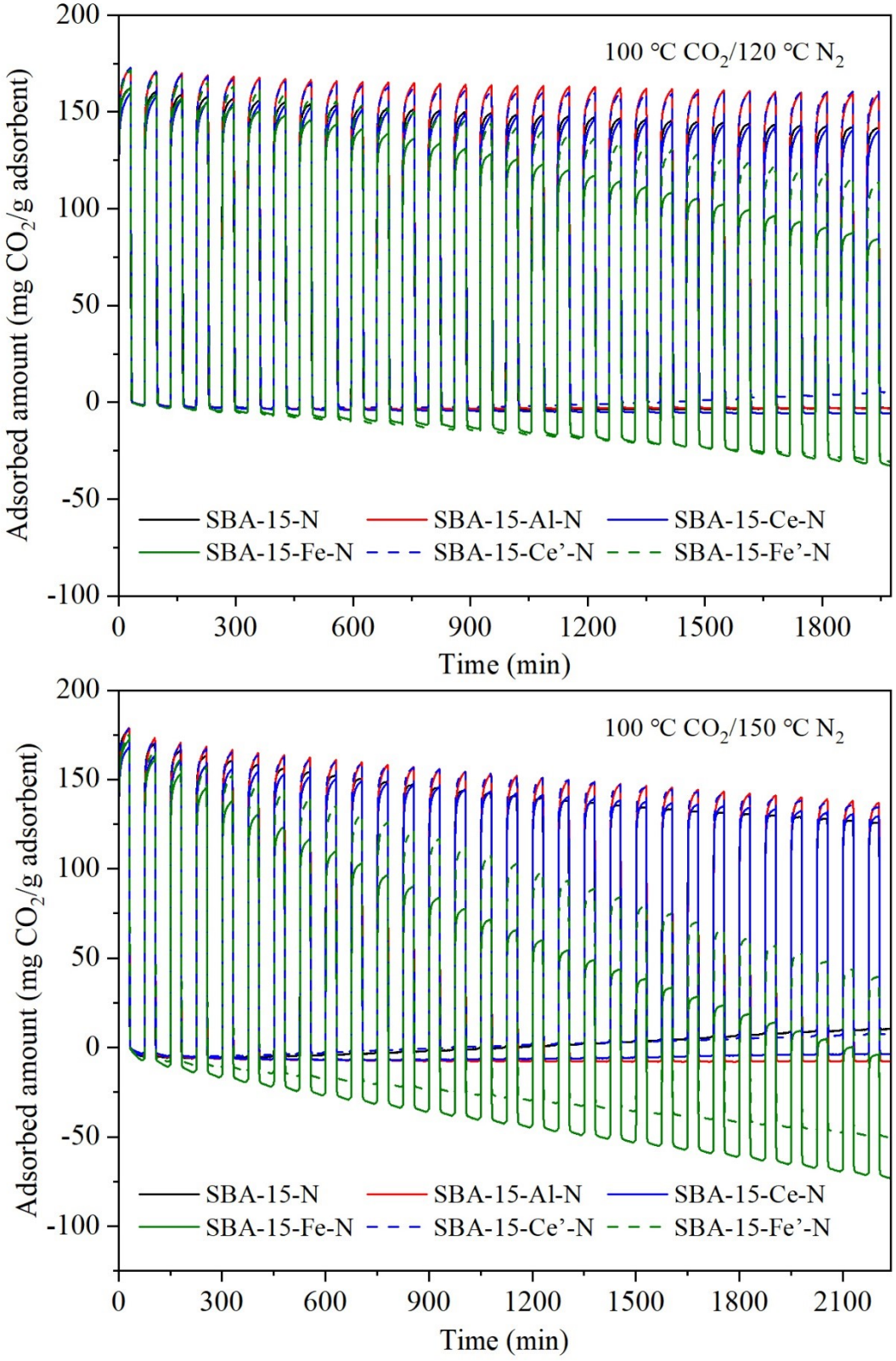

171

172 **Figure S12. TGA cycle sorption–desorption isotherms under different conditions**

173

3 Supporting tables

Table S1. Comparison of adsorption abilities and cyclic stabilities of solid amine adsorbents.

Sample	Anti-urea modification	Adsorption temperature	Desorption temperature	CO_2 uptake before modification	CO_2 uptake after modification	Cyclic stability before modification	Cyclic stability after modification	Ref.
		℃	℃	mg/g	mg/g			
PEI/SBA-15	Metal incorporation	100	120	184.24	185.43	10.8% decay after 30 cycles	6.2% decay after 30 cycles	This work
		100	150			35.9% decay after 30 cycles	19.0% decay after 30 cycles	
0.16-HBP	Hydroxylation	25	85	231.44	178.20	54.6% decay after 20 cycles	No decay after 20 cycles	[5]
PEI/CSH	Metal incorporation	90	120	/	198	/	1.9% decay after 10 cycles	[6]
		90	150			/	48.0% decay after 10 cycles	
PEI/SBA-15	Metal incorporation	75	130	77.5	67.5	42.9% decay after 50 cycles	5.2% decay after 50 cycles	[7]
EDA/zeolite	H_2O co-adsorption	40	130	145.2	70.4	74.3% decay after 20 cycles	21.4% decay after 20 cycles	[8]
PEI/Silica	Cross-linking agents	100	130	140	121	83.1% decay after 40 cycles	39.0% decay after 40 cycles	[9]
PEI/Silica	Cross-linking agents	40	130	209	154	55.8% decay after 15 cycles	18.8% decay after 15 cycles	[10]

PEI/Silica	Cross-linking agents	40	150	114	101	57.7% decay after 5 cycles	21.7% decay after 5 cycles	[11]
PEI/Silica	Hydroxylation	40	120	132	96.8	63.3% decay after 50 cycles	No decay after 50 cycles	[12]
PEI/Silica	/	45	110	/	76	/	12.0% decay after 10 cycles	[13]
PEI/Silica	/	105	100	/	132	/	7.3% decay after 20 cycles	[14]
PEI/Silica	/	75	110	/	107	/	No decay after 8 cycles	[15]
PEI/Silica	/	75	105	/	215	/	4.9% decay after 10 cycles	[16]
PEI/Silica	/	25	100	/	155	/	12.7% decay after 5 cycles	[17]
APTES/Silica	/	25	110	/	54.1	/	5.7% decay after 5 cycles	[18]

Table S2. Pore characteristics and element contents of SBA-15, metal-incorporated silica, and amine-impregnated adsorbents.

Sample	S_{BET}	V_{BJH}	D_{BJH}	N content	Amine loading	n_{metal} : n_{SiO2} [a]	m_{metal} : m_{SiO2} [a]
	m^2/g	cm^3/g	nm	wt.%	wt.%	mol %	wt. %
SBA-15	481.38	1.322	8.91	0.03	/	/	/
SBA-15-Al	475.62	1.281	8.61	0.01	/	3.33	1.50
SBA-15-Ce	458.22	1.211	8.46	0.00	/	3.33	7.78
SBA-15-Fe	470.59	1.278	8.92	0.00	/	3.33	3.11
SBA-15-Ce’	476.23	1.312	9.07	0.03	/	0.64	1.50
SBA-15-Fe’	476.44	1.290	8.69	0.01	/	1.61	1.50
SBA-15-N	6.57	0.036	19.07	17.27	52.96	/	/
SBA-15-Al-N	3.14	0.012	13.20	18.93	58.42	3.33	1.50
SBA-15-Ce-N	3.69	0.014	14.88	16.87	52.40	3.33	7.78
SBA-15-Fe-N	5.63	0.029	18.54	16.55	51.78	3.33	3.11
SBA-15-Ce’-N	3.33	0.011	14.19	17.85	55.08	0.64	1.50
SBA-15-Fe’-N	3.88	0.015	13.53	17.96	55.33	1.61	1.50

[a] This referred to the proportion added during preparation.

185 **Table S3. Actual metal contents of amine-impregnated adsorbents.**

Sample	Al content	Ce content	Fe content	Al content [a]	Ce content [a]	Fe content [a]
	wt. %	wt. %	wt. %	mol/g adsorbent	mol/g adsorbent	mol/g adsorbent
SBA-15-N	N.D.	N.D.	N.D.	N.D.	N.D.	N.D.
SBA-15-Al-N	0.455	N.D.	N.D.	0.017	N.D.	N.D.
SBA-15-Ce-N	N.D.	2.21	N.D.	N.D.	0.021	N.D.
SBA-15-Fe-N	N.D.	N.D.	1.02	N.D.	N.D.	0.018
SBA-15-Ce'-N	N.D.	0.409	N.D.	N.D.	0.004	N.D.
SBA-15-Fe'-N	N.D.	N.D.	0.468	N.D.	N.D.	0.008

186 [a] This was calculated by Me content (wt. %).

Reference

[1] Lin L, Han S, Meng F, Li J, Chen K, Hu E, Jiang J, The influence of pore size and pore structure of silica-based material on the amine-modified adsorbent for CO2 capture[J]. Separation and Purification Technology, 2024, 340.

[2] Danish M, Parthasarthy V, Al Mesfer M K, CO2 capture using activated carbon synthesized from date stone: breakthrough, equilibrium, and mass-transfer zone[J]. Carbon Letters, 2021, 31(6): 1261-1272.

[3] Wu J, Zhu X, Yang F, Ge T, Wang R, Easily-synthesized and low-cost amine-functionalized silica sol-coated structured adsorbents for CO2 capture[J]. Chemical Engineering Journal, 2021, 425.

[4] Wilfong W C, Kail B W, Howard B H, Wang Q, Shi F, Ji T, Gray M L, Steam-Stable Basic Immobilized Amine Sorbent Pellets for CO2 Capture Under Practical Conditions[J]. ACS Applied Materials & Interfaces, 2019, 11(41): 38336-38346.

[5] He H, Tang H, Chen X, Hou X, Zhou X, Chen H, Wu S, Wang S, Structure Design of Low-Temperature Regenerative Hyperbranched Polyamine Adsorbent for CO2 Capture[J]. Langmuir, 2018, 34(47): 14169-14179.

[6] Qu F, Yan F, Shen X, Li C, Chen H, Wang P, Zhang Z, Novel PEI@CSH adsorbents derived from coal fly ash enabling efficient and in-situ CO2 capture: The anti-urea mechanism of CSH support[J]. Journal of Cleaner Production, 2022, 378.

[7] Li K M, Lu L, Xu Y R, Jia S Y, Zhang Z Q, Qi Z B, Wei S Y, The use of metal nitrate-modified amorphous nano silica for synthesizing solid amine CO2 adsorbents with resistance to urea linkage formation[J]. International Journal of Greenhouse Gas Control, 2021, 106.

[8] Kim C, Cho H S, Chang S, Cho S J, Choi M, An ethylenediamine-grafted Y zeolite: a highly regenerable carbon dioxide adsorbent via temperature swing adsorption without urea formation[J]. Energy & Environmental Science, 2016, 9(5): 1803-1811.

[9] Jeon S, Min J, Kim S H, Lee K B, Introduction of cross-linking agents to enhance the performance and chemical stability of polyethyleneimine-impregnated CO2 adsorbents: Effect of different alkyl chain lengths[J]. Chemical Engineering Journal, 2020, 398: 125531.

[10] Jeon S, Jung H, Kim S H, Lee K B, Double-Layer Structured CO2 Adsorbent Functionalized with Modified Polyethyleneimine for High Physical and Chemical Stability[J]. ACS Applied Materials & Interfaces, 2018, 10(25): 21213-21223.

[11] Jung H, Jeon S, Jo D H, Huh J, Kim S H, Effect of crosslinking on the CO_2 adsorption of polyethyleneimine-impregnated sorbents[J]. Chemical Engineering Journal, 2017, 307: 836-844.

[12] Choi W, Min K, Kim C, Ko Y S, Jeon J W, Seo H, Park Y-K, Choi M, Epoxide-functionalization of polyethyleneimine for synthesis of stable carbon dioxide adsorbent in temperature swing adsorption[J]. Nature Communications, 2016, 7(1).

[13] Sanz-Pérez E S, Dantas T C M, Arencibia A, Calleja G, Guedes A P M A, Araujo

A S, Sanz R, Reuse and recycling of amine-functionalized silica materials for CO_2 adsorption[J]. Chemical Engineering Journal, 2017, 308: 1021-1033.
[14] Kishor R, Ghoshal A K, Polyethylenimine Functionalized As-Synthesized KIT-6 Adsorbent for Highly CO_2/N_2 Selective Separation[J]. Energy & Fuels, 2016, 30(11): 9635-9644.
[15] Guo X, Ding L, Kanamori K, Nakanishi K, Yang H, Functionalization of hierarchically porous silica monoliths with polyethyleneimine (PEI) for CO_2 adsorption[J]. Microporous and Mesoporous Materials, 2017, 245: 51-57.
[16] Chen C, Xu H, Jiang Q, Lin Z, Rational design of silicas with meso-macroporosity as supports for high-performance solid amine CO_2 adsorbents[J]. Energy, 2021, 214.
[17] Rao N, Wang M, Shang Z, Hou Y, Fan G, Li J, CO_2 Adsorption by Amine-Functionalized MCM-41: A Comparison between Impregnation and Grafting Modification Methods[J]. Energy & Fuels, 2018, 32(1): 670-677.
[18] Li X, Wang Z, Feng R, Huang J, Fang Y, CO2 capture on aminosilane functionalized alumina-extracted residue of catalytic gasification coal ash[J]. Energy, 2021, 221: 119642.